nature geoscience

Review article

https://doi.org/10.1038/s41561-024-01617-9

Variation in slip behaviour along megathrusts controlled by multiple physical properties

Received: 31 October 2023

Accepted: 21 November 2024

Published online: 8 January 2025

Check for updates

Dan Bassett[1] ✉, Donna J. Shillington[2], Laura M. Wallace[3,4,5] & Julie L. Elliott[6]

Megathrusts, faults at the plate interface in subduction zones, exhibit substantial spatiotemporal variability in their slip behaviour. Many previous attempts to discern the physical controls on their slip behaviour have focused on individual variables, often associated with the physical properties of either the subducting plate (for example, its age and roughness) or the overriding plate (for example, its thickness and rigidity). Such studies, which are often location-specific or focused on single variables, have fuelled contrasting views on the relative importance of various physical properties on megathrust slip behaviour. Here we synthesize observations of the Alaska, Hikurangi and Nankai subduction zones to ascertain the main causes of the well-documented changes in interseismic coupling and earthquake behaviour along their megathrusts. In all three cases, along-trench changes in the distribution of rigid crustal rocks in the forearc, the geometry of the subducting slab and the upper-plate stress state drive considerable variability in the downdip width of the seismogenic zone. The subducting plate is systematically rougher in creeping regions, with fault-zone heterogeneity promoting a mixture of moderate to large earthquakes, near-trench seismicity and slow-slip events. Smoother subducting plate segments (with thicker sediment cover) are more strongly correlated with deep interseismic coupling and great (>M_w 8) earthquakes. In the three regions considered, there is no one dominant variable. Rather, we conclude that several physical properties affecting the dimensions and heterogeneity of megathrusts collectively explain observed along-trench transitions in slip behaviour at these subduction zones, and potentially at many other subduction zones worldwide.

Resolving the physical processes that lead to great (moment magnitude > (M_w) 8) subduction earthquakes is a societally important issue with substantial scientific challenges. The long recurrence intervals of the largest earthquakes and the specific environmental conditions required to preserve geological evidence for past earthquakes mean that the absence of great earthquakes in historical or palaeoseismic records is not a reliable indicator that they cannot occur in a particular region[1]. Geodetic measurements of surface deformation can provide a view of contemporary interseismic strain accumulation on megathrusts. However, offshore constraints on crustal deformation are absent in most subduction zones, and it is possible that temporal variations in interseismic coupling occur throughout the earthquake cycle[2]. Consequently, the most informative approaches involve the joint interpretation of geodetic data with palaeoseismic and historical constraints, within a data-rich environment where known physical characteristics of subduction zones can be related to fault-slip behaviour[3,4].

A full list of affiliations appears at the end of the paper. ✉e-mail: d.bassett@gns.cri.nz

https://doi.org/10.1038/s41561-024-01617-9

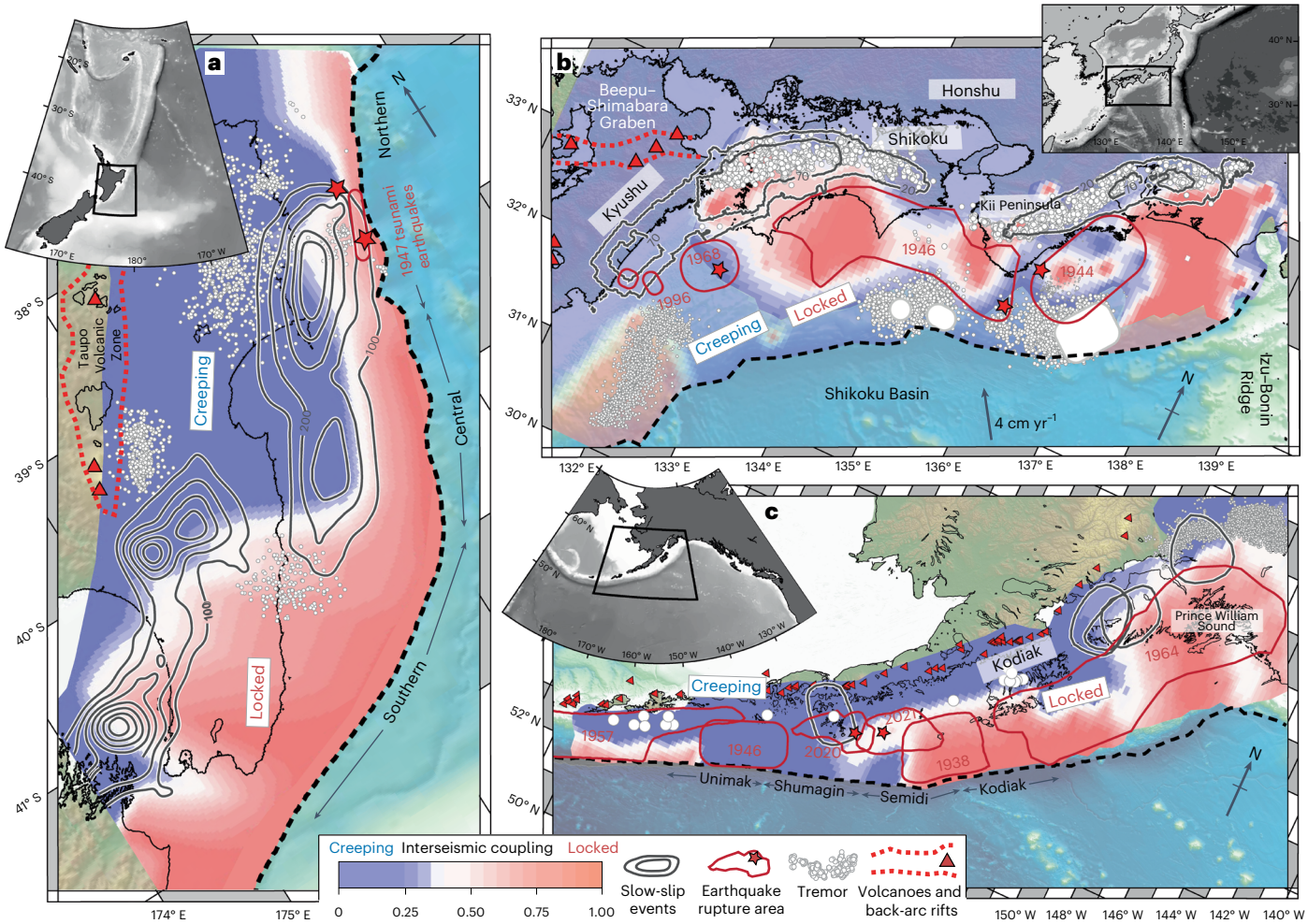

Fig. 1 | Spatial variability in slip behaviour. Maps show the degree of interseismic coupling and the distribution of large earthquakes (red ellipses), tremor (white dots) and slow-slip events (grey contours). **a**, Hikurangi margin showing sharp transitions in the strength of interseismic coupling and the cumulative distribution (2002–2014) of SSEs[19,24,112–114]. **b**, Nankai Trough showing spatial variability in the up- and downdip extent of interseismic coupling, earthquakes[29–31,37,38] and the sharp transition from deep interseismic coupling to creep between Shikoku and Kyushu[27]. Contours show cumulative slow slip (1994–2022)[28,39,40]. White dots and polygons mark shallow tremor and very-low-frequency earthquakes associated with shallow SSEs[35,40,89,90]. **c**, Alaska showing the gradual increase in the width and landward extent of the locked seismogenic zone[41–49,53–57]. Grey ellipses represent individual SSEs[45,46,48]. Note: differences in near-trench coupling are not well constrained and reflect the contrasting availability of seafloor geodetic data (no data in Alaska and Hikurangi) and different assumptions made in the geodetic data inversions for coupling.

Many of the conceptual frameworks and theories proposed to account for spatial changes in slip behaviour involve physical properties of the subduction zone and are commonly attributed to either the subducting or overriding plates. Sediments, basement topography, plate age and fluids carried into the subduction zone by the subducting plate are proposed to control plate boundary frictional properties, temperature, slab geometry, fault-zone structure and heterogeneity, and the abundance and distribution of fluids (for example, refs. 3–12). The rigidity, thickness, stress state and permeability of the overriding plate are proposed to influence the distribution of fluids, the ability of the surrounding crust to accrue elastic strain between earthquakes and earthquake dynamics when this strain is released[9,13–17].

Subduction zones with well-documented along-strike variations in earthquake behaviour are ultimately the best locales to isolate the physical parameters that vary in concert with slip behaviour. In this Review, we present a comparison of three subduction zones with the largest well-documented along-strike changes in coupling and earthquake behaviour: the Hikurangi, Alaska and Nankai subduction zones. We exploit these along-strike variations in slip behaviour to illuminate common properties that can explain subduction earthquake occurrence and interseismic coupling across each of these regions and discuss the interplay between these variables.

Along-strike variations in slip behaviour

Along New Zealand's Hikurangi margin, the megathrust undergoes an abrupt transition from deep (~30 km) interseismic coupling and deep (25–40 km), long-duration (1–2 year), slow-slip events (SSEs) in the south, to low interseismic coupling and shallow (<15 km), short-duration (several weeks) SSEs along the central and northern segments (Fig. 1a)[18–21]. While no historic great ($\geq M_w$ 8.0) earthquakes have occurred along the Hikurangi margin, coastal deformation and tsunami deposits identify 10 possible subduction earthquakes over 7,000 years, with the deeply locked southern Hikurangi margin rupturing in $>M_w$ 8.0 earthquakes every 335–655 years and at least 4 events rupturing the southern and central segments[22,23]. Two M_w ~7 tsunami earthquakes ruptured the shallow, mostly creeping sections of the northern Hikurangi margin in 1947[24].

A strikingly similar transition in slip behaviour to that in Hikurangi occurs between Shikoku and Kyushu in southwestern Japan (Fig. 1b). The Nankai megathrust beneath Shikoku and the Kii Peninsula is characterized by deep interseismic coupling[25–28] (analogous to southern

Hikurangi) and produced great earthquakes in 1944 (M_W 8.1) and 1946 (M_W 8.6)[29–31]. This region of deep interseismic coupling is flanked updip and downdip by SSEs, including an ~600 km long, 25–40 km deep band of episodic tremor and slip (ETS) located downdip of the seismogenic zone[32–36]. By contrast, the megathrust offshore Kyushu is dominated by interseismic creep[25,27] (analogous to north Hikurangi), typically producing moderate- to large-magnitude earthquakes such as in 1968 (M_W 7.5)[37] and 1996/1997 (M_W 6–7)[38], with no historical record of M 8 earthquakes. Beneath Kyushu, the ETS band observed elsewhere along Nankai Trough is not observed, and tremor and low-frequency earthquakes occur predominantly offshore between ~20 km depth and the trench[28,39,40].

Along the Alaska subduction zone, the area of the megathrust characterized by high interseismic coupling and the area and magnitude of historic megathrust earthquakes decrease westward along the margin[41–43]. In the northeast, the 1964 M 9.2 Alaska earthquake ruptured ~800 km along strike, and the factor-of-two reduction in the landward extent of co-seismic slip between Prince William Sound (300 km) and Kodiak Island (150 km) is consistent with the spatial distribution of high interseismic coupling and the location of SSEs and non-volcanic tremor downdip of the seismogenic zone (Fig. 1c)[44–52]. High interseismic coupling persists between the Kodiak and Semidi Islands, coinciding with the 1938 M 8.3 earthquake asperity[53,54]. Southwest across the Semidi and Shumagin segments, further reductions in both the strength and downdip width of plate coupling are consistent with the downdip extent of co-seismic slip in the 2021 M 8.2 Chignik and 2020 M 7.8 Shumagin earthquakes[43,55,56]. Although limited geodetic data suggest creep predominates within the Unimak segment (Fig. 1c), this region produced a tsunami earthquake (M_w 8.6) in 1946, generating the largest tsunami recorded along the Alaska trench[57].

Subduction inputs, fault-zone heterogeneity and fluids

The roughness and stratigraphic cover of the incoming plate are key properties impacting the structure, mechanics and composition of the outer forearc, the thickness and roughness of the megathrust fault and the distribution of lithologies and fluids along it[3–6,58]. Residual bathymetric maps of seafloor topography (Fig. 2) and seismic images of subseafloor structure (Fig. 3) show all three regions exhibit a general transition from a smoother, more thickly sedimented and homogeneous incoming plate in regions of high interseismic coupling and large earthquakes to a rougher, more heterogeneous plate in creeping regions. These differences reflect variability in topographic roughness on the incoming plate from seamount subduction and bending faulting[3,6,59] and the thickness of sediment entering the trench, which can blanket this topography, thereby promoting homogeneity[60–62].

Seismic reflection images traversing the deeply coupled south Hikurangi margin and the Semidi segment in Alaska reveal thick sequences of subducting sediment (Fig. 3b–d). These sequences blanket small-scale roughness and allow the megathrust to localize along a discrete stratigraphic interval, providing a smooth and lithologically homogeneous megathrust at depth[60–62]. Adjacent regions of lower coupling along the Shumagin segment in Alaska and the central and northern Hikurangi margin are characterized by lower ratios of subducting sediment thickness to plate roughness (Fig. 3a–c). This results in a rougher and more structurally complex fault zone localized along the compositionally heterogeneous top of the subducting crust at depth[6,62,63]. At Nankai, the incoming plate is roughest within the central province of Shikoku Basin, due to a relict spreading centre and the Kinan seamount chain, and in western Nankai Trough where the remnant Kyushu–Palau ridge subducts beneath Kyushu (Fig. 2c)[64–66]. Although the bathymetric expression of the Kyushu–Palau Ridge is ~80 km wide, seismic reflection data reveal subsurface roughness extending ~60 km farther beneath Shikoku Basin (Fig. 3e). Extrapolating the extent of the Kyushu–Palau roughness beneath the forearc (dashed red line in Fig. 2b) coincides with an abrupt reduction in topographic gradient across the outer forearc and the region of weak interseismic coupling, shallow SSEs and tremor offshore Kyushu[26,40,66]. These observations suggest incoming plate roughness may contribute to reductions in interseismic coupling in all three subduction zones.

The subducting plate delivers fluids into the subduction zone in the pores of crust and overlying sediments[5,67,68] and as hydrous minerals in the oceanic crust and mantle[69,70]. These fluids can promote SSEs and creep through development of elevated pore-fluid pressure[4] and modify the frictional behaviour of the oceanic crust and mantle[71]. Where a relatively thick sediment section subducts in Nankai and Alaska, the shallowest part of the megathrust is characterized by elevated pore-fluid pressures[61,72,73] and at Nankai experiences shallow SSEs[35]. Dewatering, compaction and metamorphism of these sediments may promote formation of a coherent asperity at depth[74]. In the creeping portions of the Alaska, Nankai and Hikurangi subduction zones, extensive upper-crustal hydration is observed[66,67,75,76], with irregularly distributed sediments with inferred high pore-fluid pressure also observed in Hikurangi[75,77,78]. Elevated pore-fluid pressures may promote creep through reduction of effective normal stress on the megathrust and, at greater depth, may lead to zones of friction associated with deep ETS[13,79].

A more thickly sedimented and homogeneous plate boundary is thought to produce a uniform distribution of stressing rate accumulation on a locked megathrust, thereby promoting interseismic coupling and stress accumulation for centuries, larger rupture patches and larger earthquakes[3,80]. Structurally complex faults, lithological heterogeneity and mixed mechanical and frictional properties, by contrast, may promote a greater mix of slow and fast earthquake phenomena and shallow SSEs and/or creep[6,62,81,82]. We note that near-trench tsunamigenic earthquakes in Hikurangi[24] and Alaska[54,60] both occurred near large subducting topographic relief[60,83]. This may reflect mixed mechanical properties resulting in rate-weakening asperities emerging at shallower depth. The corollary is rough incoming plates may result in smaller and more isolated asperities, which may contribute to the mixture of SSEs and moderate to large (M 6–7) earthquakes observed at typical seismogenic zone depths (~10–30 km).

Upper-plate structure, rigidity and stress state

The crustal-scale architecture, rigidity and stress state of the overthrusting plate impacts a range of processes governing fault-zone drainage and the distribution of fluids along/above the megathrust[5,84], the distribution and rigidity of materials capable of accumulating elastic strain[16,85] and the position of frictional transitions or segment boundaries that potentially limit the dimensions of the seismogenic zone[15]. All three regions exhibit along-strike transitions in upper-plate structure and stress state, which appear related to transitions in megathrust slip behaviour.

In southwestern Japan, high-resolution two-dimensional and three-dimensional seismic velocity models reveal sharp contrasts in upper-plate structure between the lithified and consolidated rocks of the inner forearc[86,87] and the younger, actively deforming and accreted material within the accretionary prism. The location of this dynamic backstop is well correlated with a profound change in the morphology of the forearc wedge (Fig. 2b) and varies markedly in position along Nankai Trough, occurring ~50 km from the trench offshore and northeast of Kii Peninsula, but 95–115 km from the trench offshore Cape Muroto and Kyushu (Fig. 4b)[86,88]. Intriguingly, the backstop appears to separate contrasting domains of shallow megathrust slip behaviour. Large earthquakes are focused downdip of the backstop[86], with slow earthquake phenomena accommodating strain updip of the backstop, beneath the outer forearc[35,40,89,90].

A similar observation is made along the Alaska Peninsula. Changes in forearc morphology and velocity are associated with the crustal backstop[60,61] and terrane boundaries within the inner forearc[91,92]. The

https://doi.org/10.1038/s41561-024-01617-9

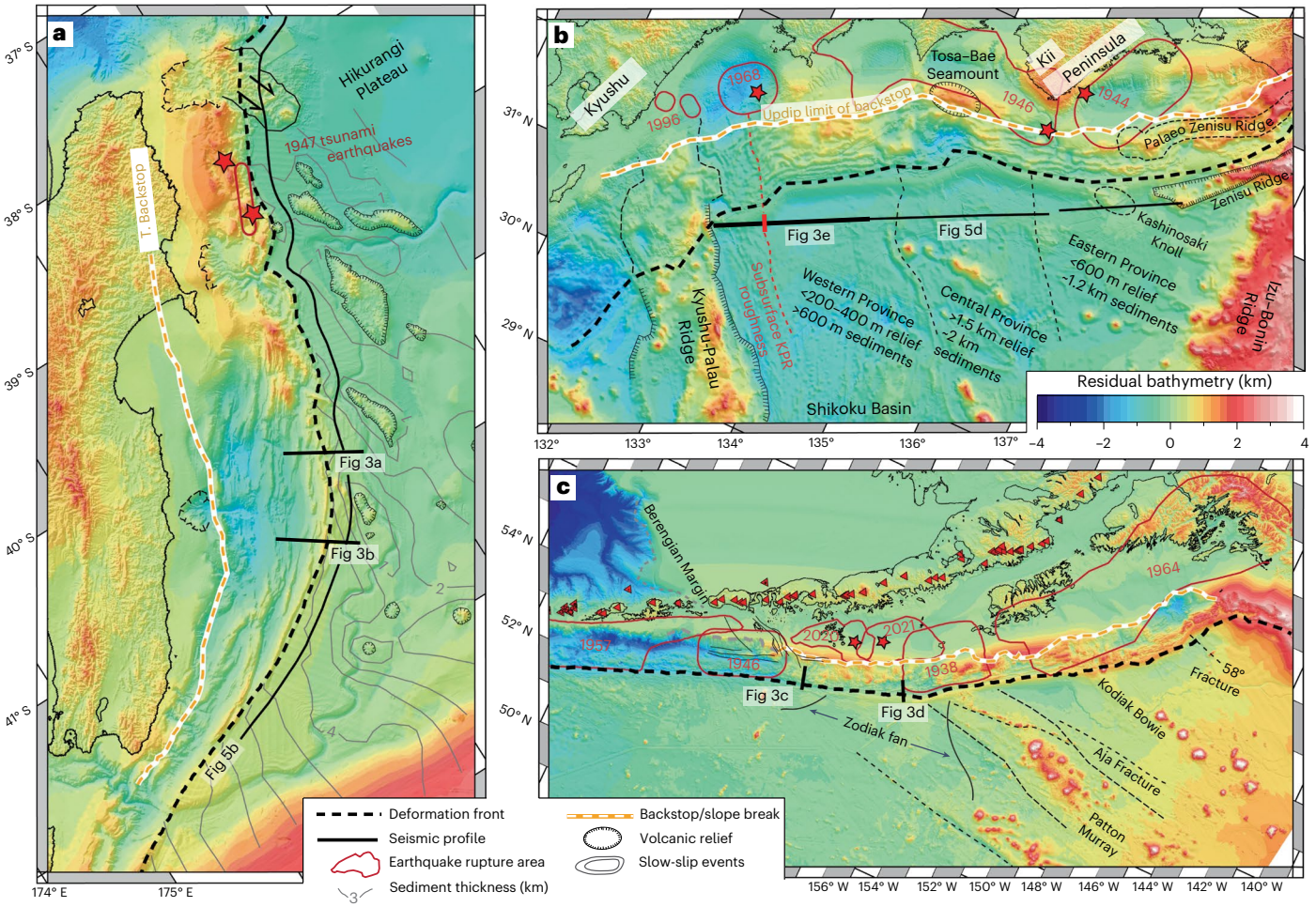

Fig. 2 | Incoming plate roughness and trench-slope morphology. a–c, Residual bathymetry[115] for Hikurangi (**a**), Nankai Trough (**b**) and Alaska (**c**). Residual bathymetry represents the deviation from average trench-normal topography. Seaward of the trench, these maps reveal spatial variability in sediment thickness and the roughness/fabric of the subducting plate. Landward of the trench, these maps highlight the contrasts between the inner (smooth) and outer (steep, rough and heavily faulted) forearc wedge. In Hikurangi, reductions in sediment thickness (grey contours[62]) increase the seafloor expression of seamounts. In Nankai, note the solid and dashed red lines marking the observed (Fig. 3e) and extrapolated extent of seafloor roughness east of Kyushu–Palau Ridge.

updip extent of recent earthquakes rupturing the Shumagin (2020) and Semidi (2021) segments appear to coincide with the continental shelf break and terrane boundaries in the inner forearc (Fig. 2c)[55,56]. Recent results documenting aseismic after-slip suggest rate-strengthening friction updip of the 2021 M 8.2 Chignik earthquake[93]. The rupture area of the giant 1964 (M_w 9.2) earthquake is less well determined but also occurs predominantly downdip of the continental shelf break, with near-trench rupture proposed only offshore Kodiak Island and the Kenai Peninsula[47]. Near-trench slip in this location may be due to the narrow width (~30 km) of the outer wedge[94], or elevated incoming plate roughness with both the Kodiak–Bowie seamount chain and Patton Murray Ridge coinciding with regions of shallow megathrust rupture (Fig. 2c[54]).

The Hikurangi margin is similar to Alaska, exhibiting along-strike changes in the width of the frontal accretionary wedge and the distribution of geological basement terranes within the inner forearc. The crustal backstop (dashed yellow line in Fig. 4a) is located within 30 km of the deformation front at the deeply locked Southern Hikurangi margin, increasing to ~100 km along the (mostly creeping) central and northern segments[95]. These differences in geological architecture may contribute to observations of higher wave speeds, lower attenuation and lower resistivity in the upper plate overlying the southern Hikurangi margin, relative to the upper plate farther north[95–98]. Geological architecture may also impact megathrust slip behaviour, with tsunami earthquakes located where the accretionary wedge is particularly narrow along the north Hikurangi margin and the downdip extent of shallow SSEs broadly correlated with the offshore extent of the Torlesse backstop[95]. Although the absence of great earthquakes in the historical record at Hikurangi make upper-plate links uncertain, these observations may reflect similar relationships to Nankai and Alaska and suggest that upper-plate rigidity potentially impacts the distribution of shallow conditional stability along the Hikurangi margin.

One key observation in both Nankai and Hikurangi is that reductions in the depth and degree of interseismic coupling occur concurrently with a shift from long-term upper-plate transpression to upper-plate extension[14]. An upper-plate extensional stress state will increase vertical structural permeability, potentially decreasing fluid pressures within the upper plate. The rapid increases in stress with depth expected in environments with lower fluid pressure may result in a shallower frictional-to-viscous transition within the upper plate and along the megathrust[14,99]. The opposite is true for an upper plate under long-term transpression, where horizontal hydrofractures occur, fluids are more easily trapped and near-lithostatic fluid pressures produce a more gradual increase in stress with depth, potentially enabling a deeper brittle-to-viscous transition (and thus, deeper megathrust coupling and seismogenesis). Such changes in structural permeability may contribute to the along-strike changes in seismic and electrical properties discussed in the preceding paragraph[97,98]. Upper-plate

https://doi.org/10.1038/s41561-024-01617-9

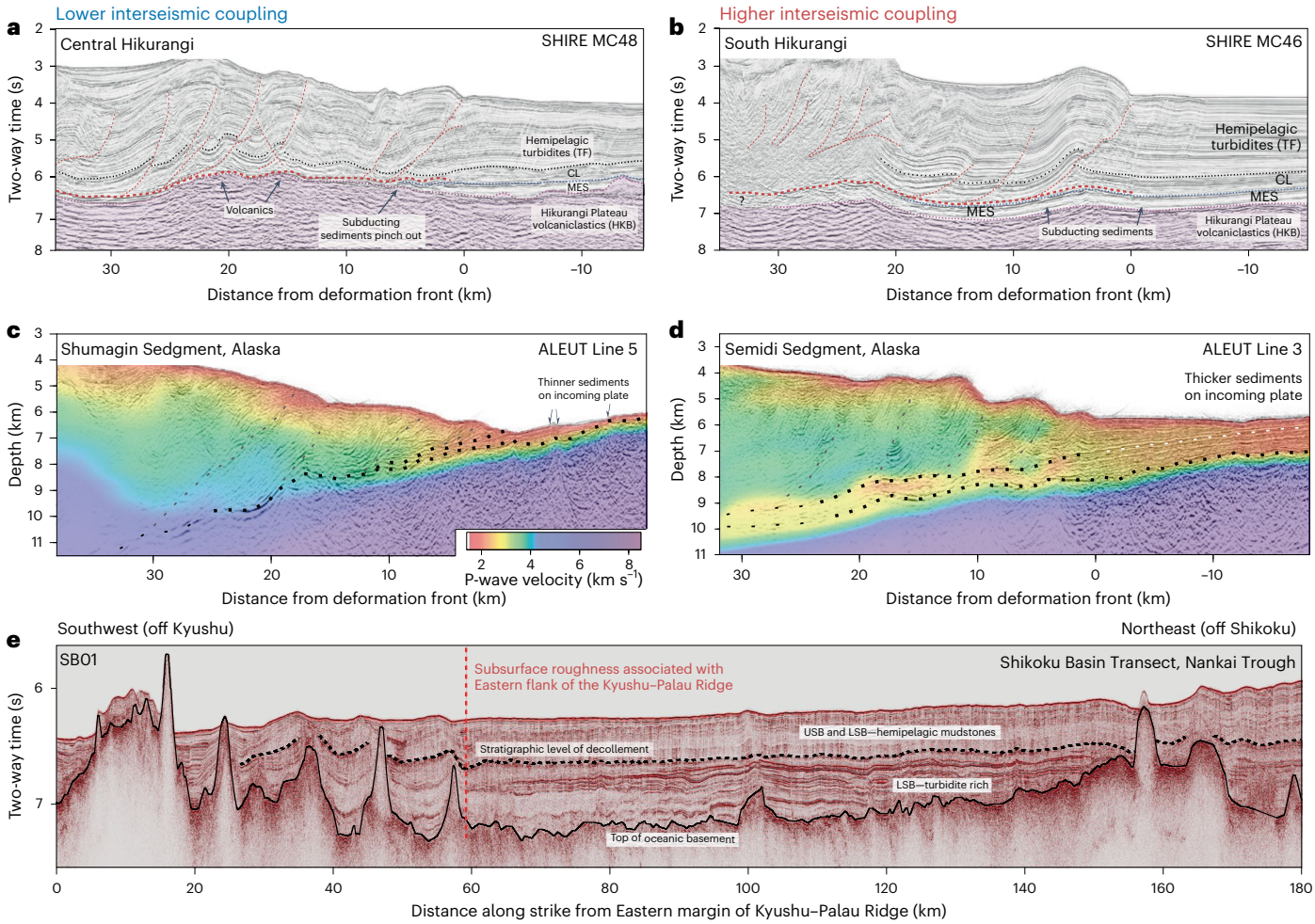

Fig. 3 | Incoming plate roughness and sediment cover. a–e, Seismic reflection images reveal along-strike changes in incoming plate roughness and sediment cover at Hikurangi (**a**,**b**), Alaska (**c**,**d**) and Nankai Trough (**e**). Regions of higher interseismic coupling (**b**,**d**) are characterized by higher ratios of subducting sediment to incoming plate roughness, resulting in a smoother and more homogeneous decollement. Regions of lower interseismic coupling (**a**,**c**) are characterized by thinner sequences of subducting sediment and/or rougher incoming plates, resulting in a rougher and more heterogeneous decollement at depth. Note the bathymetric expression of subseafloor roughness off Kyushu. This informed the spatial extent of incoming plate roughness east of Kyushu–Palau Ridge (dashed red line on Fig. 2b). Hikurangi stratigraphic nomenclature: TF, siliciclastic trench-fill sequence of hemipelagic turbidites; CL, plateau cover sequence of nannofossil chalks interbedded with tephras and clays; MES, Late Cretaceous sediments. Panels adapted with permission from: **a**,**b**, ref. 62, Geological Society of America; **c**,**d**, ref. 61, Geological Society of America.

stress state is less well resolved along the Alaska Peninsula, but seismic imaging of active normal faults suggests that upper-plate extension associated with the onset of Aleutian strain partitioning may be present in the transitional/creeping Unimak and Shumagin segments[63,100]. It should be noted the influence of fluid pressure described in the preceding sentences on the depth to the brittle/ductile transition associates high fluid pressure with a more gradual increase in stress with depth, and a greater depth to the frictional-to-viscous transition. This contrasts with the role that high fluid pressures can play in promoting aseismic creep through the reduction in effective normal stress on the megathrust (as described in: Subduction inputs, fault-zone heterogeneity and fluids).

Slab geometry and the downdip width of the seismogenic zone

In all three regions, spatial variability in the geometry of the subducting slab is a major factor driving along-strike differences in the downdip width of the seismogenic zone. Figure 4 shows the position of the downdip limit of the seismogenic zone (dashed red line), as estimated from the downdip extent of high interseismic coupling and co-seismic slip in large earthquakes.

Along the Alaska/Aleutian trench, the eastward decrease in slab dip results in the downdip width of the seismogenic zone in the Semidi segment being 50% narrower than it is farther east beneath Anchorage and Prince William Sound (Fig. 4c)[47,101]. This is highly analogous to Nankai Trough, where the complex geometry of the subducting Philippine Sea plate also results in seismogenic zone widths varying by a factor of two along strike[88](Fig. 4b). However, across the locked–unlocked transitions at Hikurangi and Nankai, reductions in interseismic coupling depth are sharper than the gradual steepening of the subducting slab[102]. In these regions, shallowing of deep SSEs, concomitant with the upper-plate stress state flipping from transpression to extension, suggest weaker coupling, and a narrower seismogenic zone may also reflect a reduction in the depth of the brittle–ductile transition[14,99]. Spatial variability in slab geometry in Alaska, Hikurangi and Nankai Trough is caused predominantly by differences in the crustal thickness and/or age of the incoming plate[103–105], but has also been shown to be locally impacted by upper-plate structure at Kii Peninsula, southwestern Japan[106].

Collectively, spatial variability in the position of the crustal backstop, slab geometry and upper-plate stress state combine to produce large changes in the downdip width of the seismogenic zone (Figs. 4 and 5).

https://doi.org/10.1038/s41561-024-01617-9

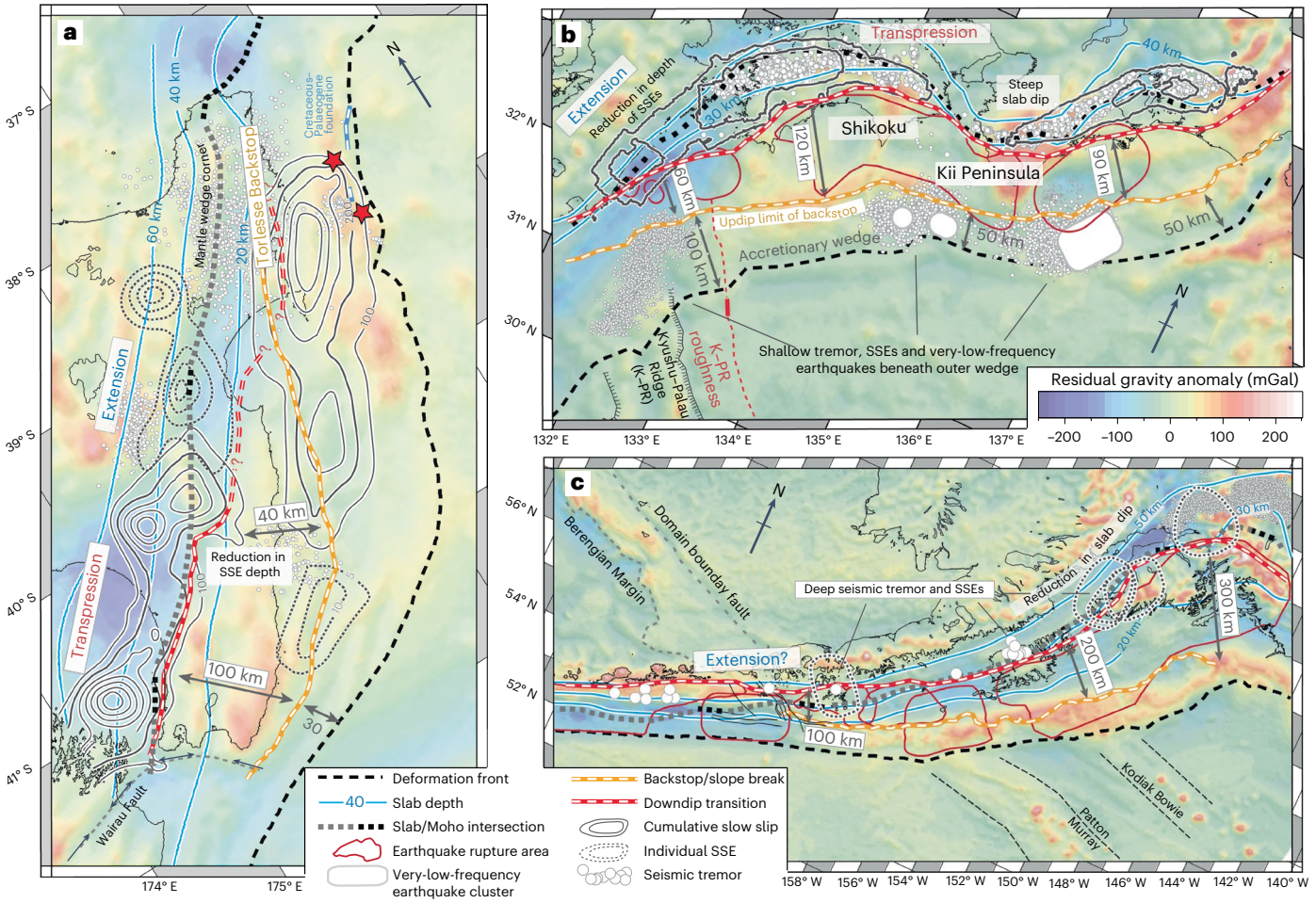

Fig. 4 | Downdip dimensions of the seismogenic zone. a–c, Maps show residual gravity[115], illustrating how spatial variability in slab geometry, upper-plate stress state and the location of margin-normal changes in upper-plate rigidity combine to produce large changes in the downdip width of the seismogenic zone. In Nankai (**b**) and Alaska (**c**), the downdip transition is well determined by recent earthquakes, SSEs and geodetic coupling models[27,43,44]. In Hikurangi (**a**), the downdip transition is estimated from interseismic coupling, deep SSEs[19,21] and surface deformation in palaeoseismic data[22]. The updip transition appears well correlated with the crustal backstop in Nankai (**b**) but is uncertain in Alaska (**c**) and Hikurangi (**a**).

In Nankai, the seismogenic zone narrows from 120 km in Shikoku to <60 km offshore Kyushu (Fig. 4b). An even larger contrast occurs along the Alaska–Aleutian trench, where the seismogenic zone progressively narrows from ~300 km beneath Prince William Sound to <100 km beneath the Shumagin Islands (Fig. 4c). In both regions, the downdip width of the seismogenic zone is broadly correlated with the strength of interseismic coupling and the magnitude of historical megathrust earthquakes (Fig. 5). In Alaska and Nankai, the width of the seismogenic zone also appears correlated with maximum co-seismic slip in historical megathrust earthquakes (dashed blue line in Fig. 5c–e). In Hikurangi, gradual south-to-north steepening of the subducting slab, the occurrence of deep SSEs at shallower depth and the landward migration of the crustal backstop appears to reduce the downdip separation of regions of shallow and deep SSEs from ~100 km across the southern Hikurangi margin to ~40 km at Cape Turnagain (Fig. 4a). This narrowing coincides with reductions in the strength of interseismic coupling, and inferences of a narrow corridor of coupling are consistent with observations of contractional strain and large ($\geq M_w$ 7) earthquakes in 1904, 1958 and 1993[21,107].

Common physical controls on transitions in slip behaviour

Figure 6 shows a cartoon illustrating the common variables that vary in concert with major along-strike changes in megathrust slip behaviour at Hikurangi, Nankai and Alaska. We suggest that these variables (related to both the subducting and overriding plates) are not necessarily independent of one another and that they can feed back on each other to influence conditions within the fault zone and subsequent megathrust slip behaviour.

The downdip width of the seismogenic zone (and the width over which interseismic coupling occurs) is strongly influenced by the geometry of the subducting slab, upper-plate stress state and the geological architecture (inner-forearc rigidity and backstop position) of the overthrusting plate. Wide zones of coupling in eastern Alaska, southern Hikurangi and Shikoku are promoted by the shallow dip of the subducting slab (Fig. 4). In adjacent regions characterized by narrower zones of coupling and/or creep, trenchward migration of the downdip limit of the seismogenic zone appears to be driven by increasing slab dip and/or a transition from transpression to extension in the upper plate, which can reduce the width of the seismogenic zone by reducing the depth of the brittle–ductile transition[14,99]. At the updip limit of the seismogenic zone, the shallow transition from unstable to stable/conditionally stable slip appears to be influenced by margin-normal transitions in upper-plate rigidity. In Alaska, a relationship is observed between the updip extent of recent earthquakes and transitions in the geological terranes within the forearc crust[92]. Nankai shows a relationship between the updip extent of earthquakes and a boundary between the forearc crust and accretionary wedge[86,88], which may also be true in Alaska and Hikurangi[61,84] but is unclear due to uncertainties in the updip extent of past earthquake ruptures. A narrower outer wedge promotes

https://doi.org/10.1038/s41561-024-01617-9

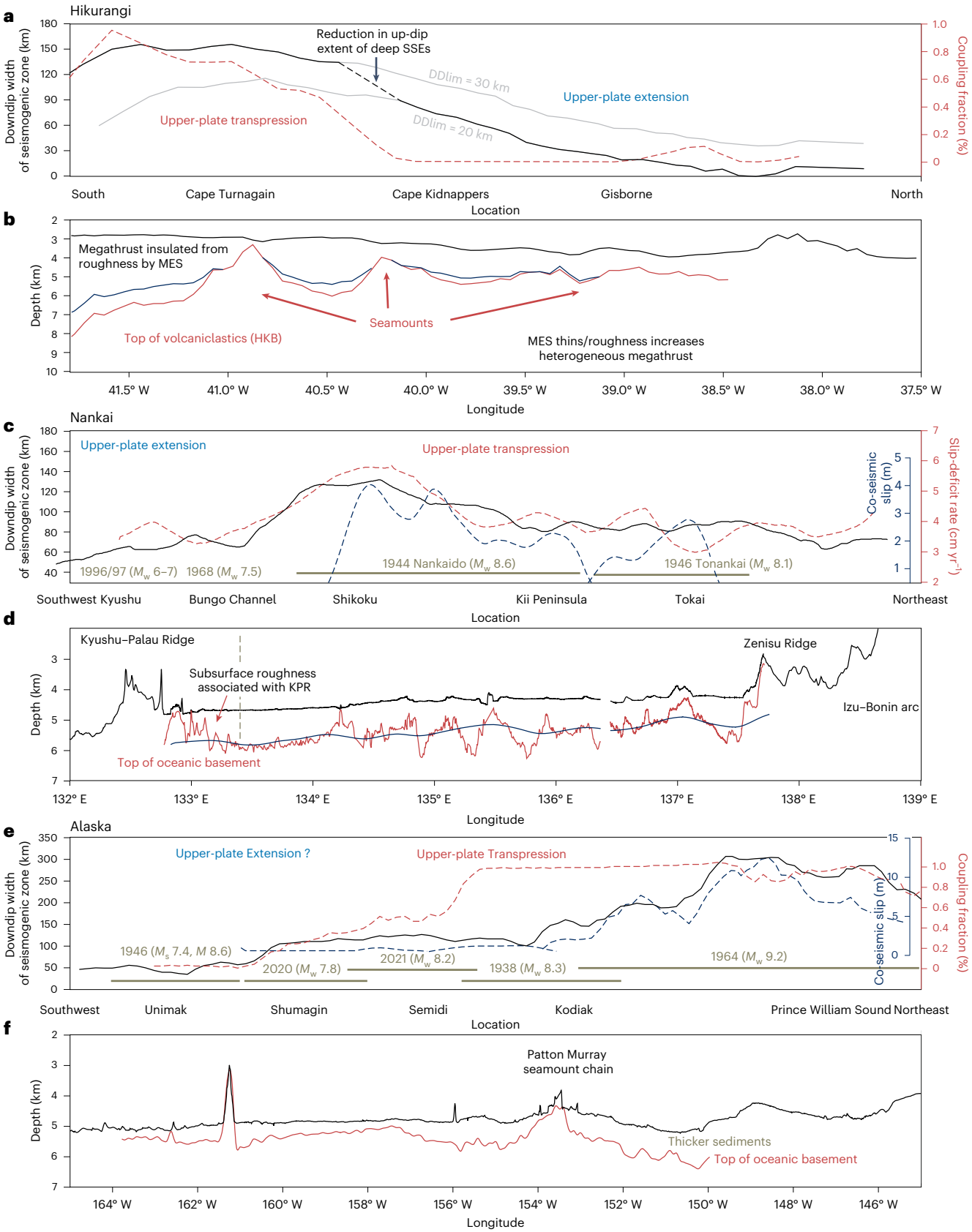

Fig. 5 | Along-strike synthesis. a–f, Margin-normal sections illustrating relationships between the downdip width of the seismogenic zone and incoming plate structure, with large earthquakes and the strength of interseismic coupling at Hikurangi (**a**,**b**), Nankai (**c**,**d**) and Alaska (**e**,**f**). In Hikurangi, the width of the seismogenic zone is estimated using a downdip transition at 30 km depth in south Hikurangi, which shallows to 20 km along the central and northern segments in line with the distribution of deep SSEs and the transition from compression to extension in the upper plate[14]. Dashed blue lines in Nankai and Alaska show the amplitude of co-seismic slip to be broadly correlated with the downdip width of the seismogenic zone. DDlim, downdip limit.

https://doi.org/10.1038/s41561-024-01617-9

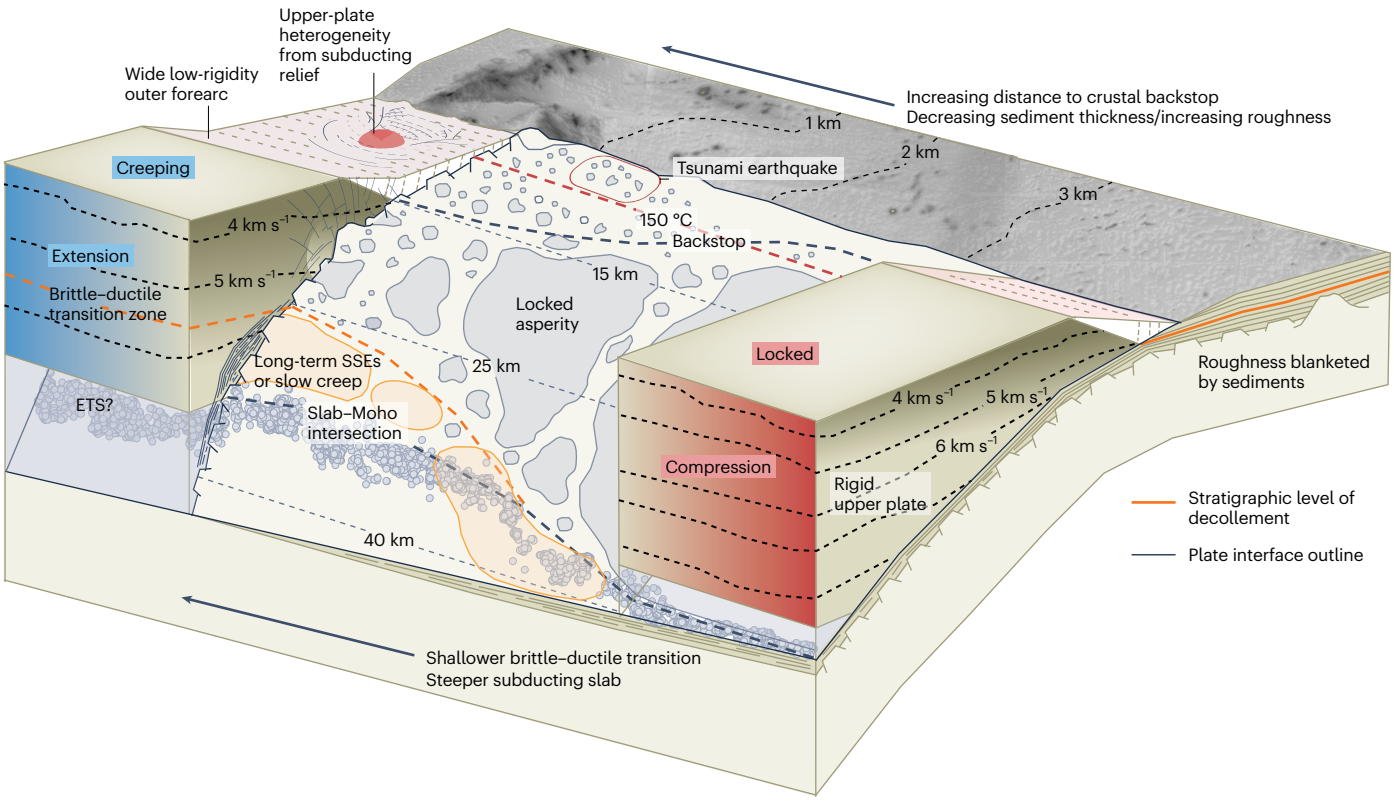

Fig. 6 | Common factors impacting slip behaviour in Alaska, New Zealand and southwestern Japan and the interplay between these. This conceptual model depicts a locked and creeping margin at each end and the characteristics that may act to push fault-slip behaviour towards either endmember. This cartoon illustrates how (1) slab geometry, upper-plate structure and stress state impact the first-order downdip dimensions of the zone of frictional coupling and (2) megathrust heterogeneity impacts the size, spacing and proportion of frictional asperities within this zone.

wide zones of coupling by placing rigid upper-plate materials nearer the deformation front, which may also increase the likelihood of near or trench-breaching rupture[94].

Within the downdip confines of the seismogenic zone, the size, distribution and frictional characteristics of asperities are strongly controlled by incoming plate roughness and the thickness and frictional properties of subducting sediment. Large asperities are promoted by smoother incoming plates and/or regions where sediments are sufficiently thick to insulate the megathrust from oceanic plate roughness. Rough incoming plates, by contrast, produce structurally and lithologically heterogeneous fault zones, with the greater mix of material properties in both the subducting and overthrusting plate leading to smaller, disconnected asperities and a mixture of both moderate to large earthquakes (~M_w 6.0–7.5), SSEs and creep at typical seismogenic zone depths[3,6,62,81,82]. Large subducting relief also imparts substantial heterogeneity in upper-plate properties as the upper plate deforms, fractures and collapses to accommodate the geometrical incompatibility of subducting topographic relief[3,67,78,108]. The downdip extent of upper-plate damage may impact shallow transitions in slip behaviour at non-accreting margins. Collectively, the heterogeneous incoming plate, fault zone and overthrusting-plate structure produced by rough incoming plates may promote the tendency for moderate to large near-trench earthquakes, but may also limit the capacity of such margins to undergo sustained, high interseismic coupling over a large area and produce great or giant earthquakes (although such events and rupture of multiple asperities cannot be ruled out).

This interpretation attributes spatial variability in interseismic coupling at Nankai, Hikurangi and Alaska to (1) slab geometry, upper-plate structure and stress state impacting the first-order downdip dimensions of the zone of frictional coupling and (2) megathrust heterogeneity impacting size, stressing rate and proportion of rate-weakening asperities within this zone. It is possible that asperities in creeping regions may be just as strong in a frictional sense, and have a higher stressing rate than those in adjacent locked regions. These asperities thereby retain the possibility of producing large earthquakes[109,110], and it is their smaller dimensions relative to the flexural rigidity of the overthrusting plate or the greater proportion of creep in surrounding areas that gives the overall impression of weaker coupling.

In summary, we identify a range of common subduction zone physical properties that vary in tandem with observed changes in slip behaviour on the Alaska, Hikurangi and Nankai megathrusts, indicating that there is no single dominant variable that controls the spatial variation in slip behaviour. Instead, we suggest that it is the collective, integrated impact of a range of factors that best explains the spatial changes in slip behaviour along these megathrusts. Although we expect that multiple interacting processes also determine the distribution of megathrust earthquakes at most subduction zones, some may be adequately explained by a single variable. Others may require an entirely different mix of properties and processes, and we acknowledge there are a range of factors that almost certainly impact megathrust slip behaviour that are not discussed here, either because we do not have the requisite data or because they are not observed to vary substantially across the transitions in slip behaviour we have considered. For example, temperature may ultimately modulate the downdip limit of the seismogenic zone in the deeply locked parts of southwest Japan[10,11], Hikurangi[99] and Alaska[111], but slab geometry and upper-plate stress state are the key factors driving spatial variability in where thermally modulated crystal plasticity sets in. Recognition of the complexity of interacting processes at the plate interface in subduction zones underscores the importance of not immediately ascribing a single variable to an entire system, but instead considering and assessing

how various properties (and the interplay between them) coalesce to influence conditions around the megathrust and its slip behaviour.

References

1. McCaffrey, R. Global frequency of magnitude 9 earthquakes. *Geology* **36**, 263–266 (2008).
2. Wang, K., Zhu, Y., Nissen, E. & Shen, Z. K. On the relevance of geodetic deformation rates to earthquake potential. *Geophys. Res. Lett.* **48**, e2021GL093231 (2021).
3. Wang, K. & Bilek, S. L. Invited review paper: fault creep caused by subduction of rough seafloor relief. *Tectonophysics* **610**, 1–24 (2014).
4. Saffer, D. M. & Wallace, L. M. The frictional, hydrologic, metamorphic and thermal habitat of shallow slow earthquakes. *Nat. Geosci.* **8**, 594–600 (2015).
5. Saffer, D. M. & Tobin, H. J. Hydrogeology and mechanics of subduction zone forearcs: fluid flow and pore pressure. *Annu. Rev. Earth Planet. Sci.* **39**, 157–186 (2011).
6. Barnes, P. M. et al. Slow slip source characterized by lithological and geometric heterogeneity. *Sci. Adv.* **6**, eaay3314 (2020).
7. Scholz, C. & Campos, J. On the mechanism of seismic decoupling and back arc spreading at subduction zones. *J. Geophys. Res. Solid Earth* **100**, 22103–22115 (1995).
8. Scholz, C. H. & Campos, J. The seismic coupling of subduction zones revisited. *J. Geophys. Res. Solid Earth* **117**, B05310 (2012).
9. Heuret, A., Conrad, C., Funiciello, F., Lallemand, S. & Sandri, L. Relation between subduction megathrust earthquakes, trench sediment thickness and upper plate strain. *Geophys. Res. Lett.* **39**, L05304 (2012).
10. Hyndman, R. & Wang, K. Thermal constraints on the zone of major thrust earthquake failure: the Cascadia subduction zone. *J. Geophys. Res. Solid Earth* **98**, 2039–2060 (1993).
11. Hyndman, R., Wang, K. & Yamano, M. Thermal constraints on the seismogenic portion of the southwestern Japan subduction thrust. *J. Geophys. Res. Solid Earth* **100**, 15373–15392 (1995).
12. Hyndman, R., Yamano, M. & Oleskevich, D. A. The seismogenic zone of subduction thrust faults. *Isl. Arc* **6**, 244–260 (1997).
13. Audet, P., Bostock, M. G., Christensen, N. I. & Peacock, S. M. Seismic evidence for overpressured subducted oceanic crust and megathrust fault sealing. *Nature* **457**, 76–78 (2009).
14. Wallace, L. M., Fagereng, Å. & Ellis, S. Upper plate tectonic stress state may influence interseismic coupling on subduction megathrusts. *Geology* **40**, 895–898 (2012).
15. Bassett, D., Sandwell, D. T., Fialko, Y. & Watts, A. B. Upper-plate controls on co-seismic slip in the 2011 magnitude 9.0 Tohoku-oki earthquake. *Nature* **531**, 92–96 (2016).
16. Sallarès, V. & Ranero, C. R. Upper-plate rigidity determines depth-varying rupture behaviour of megathrust earthquakes. *Nature* **576**, 96–101 (2019).
17. Heuret, A., Lallemand, S., Funiciello, F., Piromallo, C. & Faccenna, C. Physical characteristics of subduction interface type seismogenic zones revisited. *Geochem. Geophys. Geosyst.* **12**, Q01004 (2011).
18. Wallace, L. M., Beavan, J., McCaffrey, R. & Darby, D. Subduction zone coupling and tectonic block rotations in the North Island, New Zealand. *J. Geophys. Res.* https://doi.org/10.1029/2004JB003241 (2004).
19. Wallace, L. M., Beavan, J., Bannister, S. & Williams, C. Simultaneous long-term and short-term slow slip events at the Hikurangi subduction margin, New Zealand: implications for processes that control slow slip event occurrence, duration, and migration. *J. Geophys. Res. Solid Earth* **117**, B11402 (2012).
20. Wallace, L. M. et al. Slow slip near the trench at the Hikurangi subduction zone, New Zealand. *Science* **352**, 701–704 (2016).
21. Wallace, L. M. Slow slip events in New Zealand. *Annu. Rev. Earth Planet. Sci.* **48**, 175–203 (2020).
22. Clark, K. et al. Geological evidence for past large earthquakes and tsunamis along the Hikurangi subduction margin, New Zealand. *Mar. Geol.* **412**, 139–172 (2019).
23. Pizer, C. et al. Paleotsunamis on the southern Hikurangi subduction zone, New Zealand, show regular recurrence of large subduction earthquakes. *Seism. Rec.* **1**, 75–84 (2021).
24. Bell, R., Holden, C., Power, W., Wang, X. & Downes, G. Hikurangi margin tsunami earthquake generated by slow seismic rupture over a subducted seamount. *Earth Planet. Sci. Lett.* **397**, 1–9 (2014).
25. Wallace, L. M. et al. Enigmatic, highly active left-lateral shear zone in southwest Japan explained by aseismic ridge collision. *Geology* **37**, 143–146 (2009).
26. Yokota, Y., Ishikawa, T., Watanabe, S.-I., Tashiro, T. & Asada, A. Seafloor geodetic constraints on interplate coupling of the Nankai Trough megathrust zone. *Nature* **534**, 374–377 (2016).
27. Nishimura, T., Yokota, Y., Tadokoro, K. & Ochi, T. Strain partitioning and interplate coupling along the northern margin of the Philippine Sea plate, estimated from Global Navigation Satellite System and Global Positioning System-Acoustic data. *Geosphere* **14**, 535–551 (2018).
28. Kano, M. et al. Development of a slow earthquake database. *Seismol. Res. Lett.* **89**, 1566–1575 (2018).
29. Sagiya, T. & Thatcher, W. Coseismic slip resolution along a plate boundary megathrust: the Nankai Trough, southwest Japan. *J. Geophys. Res. Solid Earth* **104**, 1111–1130 (1999).
30. Kikuchi, M., Nakamura, M. & Yoshikawa, K. Source rupture processes of the 1944 Tonankai earthquake and the 1945 Mikawa earthquake derived from low-gain seismograms. *Earth Planets Space* **55**, 159–172 (2003).
31. Baba, T. & Cummins, P. R. Contiguous rupture areas of two Nankai Trough earthquakes revealed by high-resolution tsunami waveform inversion. *Geophys. Res. Lett.* **32**, L08305 (2005).
32. Obara, K. Nonvolcanic deep tremor associated with subduction in southwest Japan. *Science* **296**, 1679–1681 (2002).
33. Shelly, D. R., Beroza, G. C., Ide, S. & Nakamula, S. Low-frequency earthquakes in Shikoku, Japan, and their relationship to episodic tremor and slip. *Nature* **442**, 188–191 (2006).
34. Ito, Y., Obara, K., Shiomi, K., Sekine, S. & Hirose, H. Slow earthquakes coincident with episodic tremors and slow slip events. *Science* **315**, 503–506 (2007).
35. Araki, E. et al. Recurring and triggered slow-slip events near the trench at the Nankai Trough subduction megathrust. *Science* **356**, 1157–1160 (2017).
36. Yokota, Y. & Ishikawa, T. Shallow slow slip events along the Nankai Trough detected by GNSS-A. *Sci. Adv.* **6**, eaay5786 (2020).
37. Yagi, Y., Kikuchi, M., Yoshida, S. & Yamanaka, Y. Source process of the Hyuga-nada earthquake of April 1, 1968 (M_{JMA} 7.5), and its relationship to the subsequent seismicity. *J. Seismol. Soc. Jpn* **2**, 139–148 (1998).
38. Hirose, H., Hirahara, K., Kimata, F., Fujii, N. & Miyazaki, S. I. A slow thrust slip event following the two 1996 Hyuganada earthquakes beneath the Bungo Channel, southwest Japan. *Geophys. Res. Lett.* **26**, 3237–3240 (1999).
39. Tonegawa, T. et al. Spatial relationship between shallow very low frequency earthquakes and the subducted Kyushu–Palau Ridge in the Hyuga-nada region of the Nankai subduction zone. *Geophys. J. Int.* **222**, 1542–1554 (2020).
40. Yamashita, Y. et al. Migrating tremor off southern Kyushu as evidence for slow slip of a shallow subduction interface. *Science* **348**, 676–679 (2015).
41. Fournier, T. J. & Freymueller, J. T. Transition from locked to creeping subduction in the Shumagin region, Alaska. *Geophys. Res. Lett.* **34**, L06303 (2007).

42. Li, S. & Freymueller, J. T. Spatial variation of slip behavior beneath the Alaska Peninsula along Alaska–Aleutian subduction zone. *Geophys. Res. Lett.* **45**, 3453–3460 (2018).
43. Xiao, Z. et al. The deep Shumagin gap filled: kinematic rupture model and slip budget analysis of the 2020 M_w7.8 Simeonof earthquake constrained by GNSS, global seismic waveforms, and floating InSAR. *Earth Planet. Sci. Lett.* **576**, 117241 (2021).
44. Elliott, J. & Freymueller, J. T. A block model of present-day kinematics of Alaska and western Canada. *J. Geophys. Res. Solid Earth* **125**, e2019JB018378 (2020).
45. Fu, Y. & Freymueller, J. T. Repeated large slow slip events at the southcentral Alaska subduction zone. *Earth Planet. Sci. Lett.* **375**, 303–311 (2013).
46. Ohta, Y., Freymueller, J. T., Hreinsdóttir, S. & Suito, H. A large slow slip event and the depth of the seismogenic zone in the south central Alaska subduction zone. *Earth Planet. Sci. Lett.* **247**, 108–116 (2006).
47. Suito, H. & Freymueller, J. T. A viscoelastic and afterslip postseismic deformation model for the 1964 Alaska earthquake. *J. Geophys. Res. Solid Earth* **114**, B1140 (2009).
48. Wei, M., McGuire, J. J. & Richardson, E. A slow slip event in the south central Alaska Subduction Zone and related seismicity anomaly. *Geophys. Res. Lett.* **39**, L15309 (2012).
49. Brown, J. R., Prejean, S. G., Beroza, G. C., Gomberg, J. S. & Haeussler, P. J. Deep low-frequency earthquakes in tectonic tremor along the Alaska–Aleutian subduction zone. *J. Geophys. Res. Solid Earth* **118**, 1079–1090 (2013).
50. Cross, R. S. & Freymueller, J. T. Evidence for and implications of a Bering plate based on geodetic measurements from the Aleutians and western Alaska. *J. Geophys. Res. Solid Earth* **113**, B07405 (2008).
51. Peterson, C., McNutt, S. R. & Christensen, D. Nonvolcanic tremor in the Aleutian Arc. *Bull. Seismol. Soc. Am.* **101**, 3081–3087 (2011).
52. Wech, A. G. Extending Alaska's plate boundary: tectonic tremor generated by Yakutat subduction. *Geology* **44**, 587–590 (2016).
53. Estabrook, C. H., Jacob, K. H. & Sykes, L. R. Body wave and surface wave analysis of large and great earthquakes along the Eastern Aleutian Arc, 1923–1993: implications for future events. *J. Geophys. Res. Solid Earth* **99**, 11643–11662 (1994).
54. Freymueller, J. T., Suleimani, E. N. & Nicolsky, D. J. Constraints on the slip distribution of the 1938 M_W8.3 Alaska peninsula earthquake from tsunami modeling. *Geophys. Res. Lett.* **48**, e2021GL092812 (2021).
55. Elliott, J. L. et al. Cascading rupture of a megathrust. *Sci. Adv.* **8**, eabm4131 (2022).
56. Liu, C., Lay, T., Xiong, X. & Wen, Y. Rupture of the 2020 M_W7.8 earthquake in the Shumagin gap inferred from seismic and geodetic observations. *Geophys. Res. Lett.* **47**, e2020GL090806 (2020).
57. López, A. M. & Okal, E. A. A seismological reassessment of the source of the 1946 Aleutian 'tsunami' earthquake. *Geophys. J. Int.* **165**, 835–849 (2006).
58. van Rijsingen, E. et al. How subduction interface roughness influences the occurrence of large interplate earthquakes. *Geochem. Geophys. Geosyst.* **19**, 2342–2370 (2018).
59. Shillington, D. J. et al. Link between plate fabric, hydration and subduction zone seismicity in Alaska. *Nat. Geosci.* **8**, 961–964 (2015).
60. von Huene, R., Miller, J. J. & Weinrebe, W. Subducting plate geology in three great earthquake ruptures of the western Alaska margin, Kodiak to Unimak. *Geosphere* **8**, 628–644 (2012).
61. Li, J. et al. Connections between subducted sediment, pore-fluid pressure, and earthquake behavior along the Alaska megathrust. *Geology* **46**, 299–302 (2018).
62. Gase, A. C., Bangs, N. L., Van Avendonk, H. J., Bassett, D. & Henrys, S. A. Hikurangi megathrust slip behavior influenced by lateral variability in sediment subduction. *Geology* **50**, 1145–1149 (2022).
63. Bécel, A. et al. Tsunamigenic structures in a creeping section of the Alaska subduction zone. *Nat. Geosci.* **10**, 609–613 (2017).
64. Ike, T. et al. Variations in sediment thickness and type along the northern Philippine Sea Plate at the Nankai Trough. *Isl. Arc* **17**, 342–357 (2008).
65. Kodaira, S., Takahashi, N., Nakanishi, A., Miura, S. & Kaneda, Y. Subducted seamount imaged in the rupture zone of the 1946 Nankaido earthquake. *Science* **289**, 104–106 (2000).
66. Arai, R. et al. Thick slab crust with rough basement weakens interplate coupling in the western Nankai Trough. *Earth Planets Space* **76**, 73 (2024).
67. Chesley, C., Naif, S., Key, K. & Bassett, D. Fluid-rich subducting topography generates anomalous forearc porosity. *Nature* **595**, 255–260 (2021).
68. Bray, C. J. & Karig, D. E. Porosity of sediments in accretionary prisms and some implications for dewatering processes. *J. Geophys. Res. Solid Earth* **90**, 768–778 (1985).
69. Schmidt, M. W. & Poli, S. Experimentally based water budgets for dehydrating slabs and consequences for arc magma generation. *Earth Planet. Sci. Lett.* **163**, 361–379 (1998).
70. Peacock, S. M. The importance of blueschist → eclogite dehydration reactions in subducting oceanic crust. *Geol. Soc. Am. Bull.* **105**, 684–694 (1993).
71. Tulley, C., Fagereng, Å., Ujiie, K., Diener, J. & Harris, C. Embrittlement within viscous shear zones across the base of the subduction thrust seismogenic zone. *Geochem. Geophys. Geosyst.* **23**, e2021GC010208 (2022).
72. Kitajima, H. & Saffer, D. M. Elevated pore pressure and anomalously low stress in regions of low frequency earthquakes along the Nankai Trough subduction megathrust. *Geophys. Res. Lett.* **39**, L23301 (2012).
73. Hendriyana, A. & Tsuji, T. Influence of structure and pore pressure of plate interface on tectonic tremor in the Nankai subduction zone, Japan. *Earth Planet. Sci. Lett.* **558**, 116742 (2021).
74. Miller, P. K. et al. P- and S-wave velocities of exhumed metasediments from the Alaskan subduction zone: implications for the in situ conditions along the megathrust. *Geophys. Res. Lett.* **48**, e2021GL094511 (2021).
75. Gase, A. et al. Subducting volcaniclastic-rich upper crust supplies fluids for shallow megathrust and slow slip. *Sci. Adv.* **18**, eadh0150 (2023).
76. Acquisto, T., Bécel, A., Singh, S. C. & Carton, H. Evidence of strong upper oceanic crustal hydration outboard the Alaskan and Sumatran subduction zones. *J. Geophys. Res. Solid Earth* **127**, e2022JB024751 (2022).
77. Bell, R. et al. Seismic reflection character of the Hikurangi subduction interface, New Zealand, in the region of repeated Gisborne slow slip events. *Geophys. J. Int.* **180**, 34–48 (2010).
78. Bangs, N. L. et al. Slow slip along the Hikurangi margin linked to fluid-rich sediments trailing subducting seamounts. *Nat. Geosci.* **16**, 505–512 (2023).
79. Gao, X. & Wang, K. Rheological separation of the megathrust seismogenic zone and episodic tremor and slip. *Nature* **543**, 416–419 (2017).
80. Ruff, L. J. in *Subduction Zones Part II* (eds Ruff, L. J. & Kanamori, H.) 263–282 (Springer, 1989).
81. Skarbek, R. M., Rempel, A. W. & Schmidt, D. A. Geologic heterogeneity can produce aseismic slip transients. *Geophys. Res. Lett.* **39**, L21306 (2012).
82. Shreedharan, S. et al. Frictional and lithological controls on shallow slow slip at the northern Hikurangi Margin. *Geochem. Geophys. Geosyst.* **23**, e2021GC010107 (2022).

83. Barker, D. H. et al. Geophysical constraints on the relationship between seamount subduction, slow slip, and tremor at the north Hikurangi subduction zone, New Zealand. *Geophys. Res. Lett.* **45**, 12804–12813 (2018).
84. Arnulf, A. F. et al. Physical conditions and frictional properties in the source region of a slow-slip event. *Nat. Geosci.* **14**, 334–340 (2021).
85. Byrne, D. E., Davis, D. M. & Sykes, L. R. Loci and maximum size of thrust earthquakes and the mechanics of the shallow region of subduction zones. *Tectonics* **7**, 833–857 (1988).
86. Nakanishi, A., Kodaira, S., Park, J.-O. & Kaneda, Y. Deformable backstop as seaward end of coseismic slip in the Nankai Trough seismogenic zone. *Earth Planet. Sci. Lett.* **203**, 255–263 (2002).
87. Tsuji, T., Ashi, J., Strasser, M. & Kimura, G. Identification of the static backstop and its influence on the evolution of the accretionary prism in the Nankai Trough. *Earth Planet. Sci. Lett.* **431**, 15–25 (2015).
88. Bassett, D. et al. Crustal structure of the Nankai subduction zone revealed by two decades of onshore-offshore and ocean-bottom seismic data: implications for the dimensions and slip behavior of the seismogenic zone. *J. Geophys. Res. Solid Earth* **127**, e2022JB024992 (2022).
89. Nakano, M., Hori, T., Araki, E., Kodaira, S. & Ide, S. Shallow very-low-frequency earthquakes accompany slow slip events in the Nankai subduction zone. *Nat. Commun.* **9**, 984 (2018).
90. Tamaribuchi, K., Ogiso, M. & Noda, A. Spatiotemporal distribution of shallow tremors along the Nankai Trough, southwest Japan, as determined from waveform amplitudes and cross-correlations. *J. Geophys. Res. Solid Earth* **127**, e2022JB024403 (2022).
91. Horowitz, W., Steffy, D., Hoose, P. & Turner, R. *Geologic Report for the Shumagin Planning Area, Western Gulf of Alaska. Final Report* (Minerals Management Service, 1989).
92. Shillington, D. J., Bécel, A. & Nedimović, M. R. Upper plate structure and megathrust properties in the Shumagin gap near the July 2020 *M*7.8 Simeonof event. *Geophys. Res. Lett.* **49**, e2021GL096974 (2022).
93. Brooks, B. A. et al. Rapid shallow megathrust afterslip from the 2021 *M*8.2 Chignik, Alaska earthquake revealed by seafloor geodesy. *Sci. Adv.* **9**, eadf9299 (2023).
94. Hu, Y. & Wang, K. Coseismic strengthening of the shallow portion of the subduction fault and its effects on wedge taper. *J. Geophys. Res. Solid Earth* **113**, B12411 (2008).
95. Bassett, D. et al. Crustal structure of the Hikurangi Margin from SHIRE seismic data and the relationship between forearc structure and shallow megathrust slip behavior. *Geophys. Res. Lett.* **49**, e2021GL096960 (2022).
96. Bassett, D., Sutherland, R. & Henrys, S. Slow wavespeeds and fluid overpressure in a region of shallow geodetic locking and slow slip, Hikurangi subduction margin, New Zealand. *Earth Planet. Sci. Lett.* **389**, 1–13 (2014).
97. Reyners, M., Eberhart-Phillips, D. & Bannister, S. Subducting an old subduction zone sideways provides insights into what controls plate coupling. *Earth Planet. Sci. Lett.* **466**, 53–61 (2017).
98. Heise, W. et al. Electrical resistivity imaging of the inter-plate coupling transition at the Hikurangi subduction margin, New Zealand. *Earth Planet. Sci. Lett.* **524**, 115710 (2019).
99. Fagereng, A. & Ellis, S. On factors controlling the depth of interseismic coupling on the Hikurangi subduction interface, New Zealand. *Earth Planet. Sci. Lett.* **278**, 120–130 (2009).
100. Kahrizi, A. et al. Extensional forearc structures at the transition from Alaska to Aleutian subduction zone: slip partitioning, terranes and large earthquakes. *C. R. Geosci.* **356**, 53–77 (2023).
101. Hayes, G. P. et al. Slab2, a comprehensive subduction zone geometry model. *Science* **362**, 58–61 (2018).
102. Williams, C. A. et al. Revised interface geometry for the Hikurangi subduction zone, New Zealand. *Seismol. Res. Lett.* **84**, 1066–1073 (2013).
103. Kim, Y. et al. Alaska Megathrust 2: Imaging the megathrust zone and Yakutat/Pacific plate interface in the Alaska subduction zone. *J. Geophys. Res. Solid Earth* **119**, 1924–1941 (2014).
104. Wang, K., Wada, I. & Ishikawa, Y. Stresses in the subducting slab beneath southwest Japan and relation with plate geometry, tectonic forces, slab dehydration, and damaging earthquakes. *J. Geophys. Res. Solid Earth* **109**, B08304 (2004).
105. Bassett, D. et al. Heterogeneous crustal structure of the Hikurangi Plateau revealed by SHIRE seismic data: origin and implications for plate boundary tectonics. *Geophys. Res. Lett.* **50**, e2023GL105674 (2023).
106. Arnulf, A. F. et al. Upper-plate controls on subduction zone geometry, hydration and earthquake behaviour. *Nat. Geosci.* **15**, 143–148 (2022).
107. Haines, A. J. & Wallace, L. M. New Zealand-wide geodetic strain rates using a physics-based approach. *Geophys. Res. Lett.* **47**, e2019GL084606 (2020).
108. Sun, T., Saffer, D. & Ellis, S. Mechanical and hydrological effects of seamount subduction on megathrust stress and slip. *Nat. Geosci.* **13**, 249–255 (2020).
109. Bilek, S. L. & Lay, T. Tsunami earthquakes possibly widespread manifestations of frictional conditional stability. *Geophys. Res. Lett.* **29**, 1673 (2002).
110. Wallace, L. et al. Near-field observations of an offshore M_w6.0 earthquake from an integrated seafloor and subseafloor monitoring network at the Nankai Trough, southwest Japan. *J. Geophys. Res. Solid Earth* **121**, 8338–8351 (2016).
111. Oleskevich, D., Hyndman, R. & Wang, K. The updip and downdip limits to great subduction earthquakes: thermal and structural models of Cascadia, south Alaska, SW Japan, and Chile. *J. Geophys. Res. Solid Earth* **104**, 14965–14991 (1999).
112. Todd, E. K. & Schwartz, S. Y. Tectonic tremor along the northern Hikurangi Margin, New Zealand, between 2010 and 2015. *J. Geophys. Res. Solid Earth* **121**, 8706–8719 (2016).
113. Todd, E. K. et al. Earthquakes and tremor linked to seamount subduction during shallow slow slip at the Hikurangi margin, New Zealand. *J. Geophys. Res. Solid Earth* **123**, 6769–6783 (2018).
114. Romanet, P. & Ide, S. Ambient tectonic tremors in manawatu, Cape Turnagain, marlborough, and Puysegur, New Zealand. *Earth Planets Space* **71**, 59 (2019).
115. Bassett, D. & Watts, A. B. Gravity anomalies, crustal structure, and seismicity at subduction zones: 1. Seafloor roughness and subducting relief. *Geochem. Geophys. Geosyst.* **16**, 1508–1540 (2015).

Acknowledgements

D.B. was supported by Royal Society of New Zealand Marsden Fund (MFP-GNS1902) and Catalyst: Seeding (CSG-GNS2301) grants, by the New Zealand Ministry of Business Innovation and Employment (MBIE) Endeavour Grant Ngā Ngaru Wakapuke: Building Resilience to Future Earthquake Sequences (RTVU2306) and by public research funding from the Government of New Zealand Strategic Science Investment Fund to GNS Science (contract C05X1702). D.J.S. acknowledges support from NSF award OCE-2026676. L.W. acknowledges funding support from NSF grant EAR-2121666. J.E. was supported by a US Geological Survey IPA and NSF grants EAR-2052558 and EAR- 2152253. We thank P. Henry for helpful comments.

Author contributions
All authors contributed equally to planning, data compilation, analysis and writing the manuscript.

Competing interests
The authors declare no competing interests.

Additional information
Correspondence and requests for materials should be addressed to Dan Bassett.

Peer review information *Nature Geoscience* thanks the anonymous reviewers for their contribution to the peer review of this work. Primary Handling Editors: Alireza Bahadori and Stefan Lachowycz, in collaboration with the *Nature Geoscience* team.

[1]GNS Science, Lower Hutt, New Zealand. [2]Northern Arizona University, School of Earth and Sustainability, Flagstaff, AZ, USA. [3]University of Texas Institute for Geophysics, Austin, TX, USA. [4]GEOMAR Helmholtz Centre for Ocean Research, Kiel, Germany. [5]Institute of Geosciences, Christian-Albrechts-Universität zu Kiel, Kiel, Germany. [6]Michigan State University, Department of Earth and Environmental Sciences, East Lansing, MI, USA.
✉e-mail: d.bassett@gns.cri.nz